ARTICLE

Multi-parametric analysis of 57 SYNGAP1 variants reveal impacts on GTPase signaling, localization, and protein stability

Fabian Meili,[1] William J. Wei,[2] Wun-Chey Sin,[1] Warren M. Meyers,[1] Iulia Dascalu,[2] Daniel B. Callaghan,[3] Sanja Rogic,[3,4] Paul Pavlidis,[1,3,4] and Kurt Haas[1,2,*]

Summary

SYNGAP1 is a neuronal Ras and Rap GTPase-activating protein with important roles in regulating excitatory synaptic plasticity. While many *SYNGAP1* missense and nonsense mutations have been associated with intellectual disability, epilepsy, schizophrenia, and autism spectrum disorder (ASD), whether and how they contribute to individual disease phenotypes is often unknown. Here, we characterize 57 variants in seven assays that examine multiple aspects of SYNGAP1 function. Specifically, we used multiplex phospho-flow cytometry to measure variant impact on protein stability, pERK, pGSK3β, pp38, pCREB, and high-content imaging to examine subcellular localization. We find variants ranging from complete loss-of-function (LoF) to wild-type (WT)-like in their regulation of pERK and pGSK3β, while all variants retain at least partial ability to dephosphorylate pCREB. Interestingly, our assays reveal that a larger proportion of variants located within the disordered domain of unknown function (DUF) comprising the C-terminal half of SYNGAP1 exhibited higher LoF, compared to variants within the better studied catalytic domain. Moreover, we find protein instability to be a major contributor to dysfunction for only two missense variants, both located within the catalytic domain. Using high-content imaging, we find variants located within the C2 domain known to mediate membrane lipid interactions exhibit significantly larger cytoplasmic speckles than WT SYNGAP1. Moreover, this subcellular phenotype shows both correlation with altered catalytic activity and unique deviation from signaling assay results, highlighting multiple independent molecular mechanisms underlying variant dysfunction. Our multidimensional dataset allows clustering of variants based on functional phenotypes and provides high-confidence, multi-functional measures for making pathogenicity predictions.

Introduction

The neuronal Ras and Rap-GTPase activating protein (GAP) SYNGAP1 is a 1,343 amino acid (AA) protein that contains a core GAP domain and an auxiliary C2 domain essential for its regulation of other GTPase targets including Rap, Rheb, Rab, and Rac.[1–8] As a GAP, SYNGAP1 promotes the dephosphorylation of GTP to GDP by GTPases, thereby inhibiting GTPase signaling by reducing the abundance of their active, GTP-bound form.

SYNGAP1 is one of the most abundant proteins at the post-synaptic density (PSD) complex of excitatory glutamatergic synapses.[6–8] As such, it is well poised to regulate activity-dependent cytoskeletal reconfigurations and AMPA receptor (AMPAR) trafficking associated with both long-term potentiation (LTP) and long-term depression (LTD), processes mediated by Ras and Rap, respectively.[9–12] SYNGAP1 binds to the scaffolding proteins PSD95, MUPP1, and SAP102/DLG3, and closely associates with NMDA receptors (NMDARs).[6] Synaptic innervation triggering calcium influx activates Ca^{2+}/calmodulin-dependent protein kinase II (CaMK2), which then translocates to the PSD and phosphorylates SYNGAP1, causing its dissociation from PSD scaffolding proteins.[2,3,10,13–15] Its removal causes local increased Ras activity and AMPAR exocytosis mediating LTP.[12,16] Ras-ERK signaling also promotes expression of immediate early-response genes by activating CREB.[17–20] SYNGAP1 is also implicated in LTD, due to its regulation of Rab5 and Rap1.[3,16,21] In contrast to phosphorylation by CaMK2, phosphorylation of SYNGAP1 by the protein kinases CDK5 and PLK2 shifts its affinity and GAP activity from Ras to Rap, a GTPase that induces AMPAR endocytosis by activating p38.[2,11,12,22–24] In addition, SYNGAP1's C2-domain is required for its RapGAP activity.[5] SYNGAP1 thus is positioned to act as a regulator of both Ras-ERK-LTP and Rap-p38-LTD signaling.

SYNGAP1 is predominantly expressed in the developing brain, where dysfunction of LTD and LTP is believed to contribute to several neurodevelopmental disorders.[25–29] Indeed, reduced function of SYNGAP1 leads to the disruption of several synaptic signaling pathways, and mutations in *SYNGAP1* (MIM: 603384) are associated with intellectual disability (ID), epilepsy, and syndromic SYNGAP encephalopathy.[30–33] *SYNGAP1* mutations have also been identified in individuals with schizophrenia and autism spectrum disorder (ASD).[34–36] SYNGAP1 dysfunction in model systems replicates disease-associated phenotypes, as a knockdown of zebrafish *syngap1* results in delayed brain development and seizure-like behavior.[37,38] Underscoring the importance of its regulation on LTP/LTD

[1]Djavad Mowafaghian Centre for Brain Health, University of British Columbia, Vancouver, BC V6T2B5, Canada; [2]Department of Cellular and Physiological Sciences, University of British Columbia, Vancouver, BC V6T1Z3, Canada; [3]Department of Psychiatry, University of British Columbia, Vancouver, BC V6T2A1, Canada; [4]Michael Smith Laboratories, University of British Columbia, Vancouver, BC V6T1Z4, Canada
*Correspondence: kurt.haas@ubc.ca
https://doi.org/10.1016/j.ajhg.2020.11.011.

balance, homozygous *Syngap1*-null mice die within a week after birth with an increase in neuronal apoptosis, while heterozygous mice have defects in LTP and social and fear conditioning and have increased basal activity levels of Rac and ERK.[39–44] Abnormal ERK activation causes epileptic seizures in mice and the Ras-ERK pathway is commonly dysregulated in chronic schizophrenia.[45–48] *Syngap1*-heterozygous hippocampal neurons also do not exhibit LTD, presumably through aberrant cofilin activation via Rac.[34,49] Overexpression of SYNGAP1 has the opposite effect and leads to elevated levels of pp38, inhibition of ERK, and a reduction of surface AMPARs.[50,51] Additionally, SYNGAP1 has been shown to regulate apoptosis, a process that, like LTD, is regulated by GSK3β.[43,52–56]

While many mutations in *SYNGAP1* are identified as pathogenic early termination/truncating variants, there is a growing number of missense variants found in individuals with ASD, ID, and other neurological/psychiatric disorders for which potential effect on protein function and contribution to disease is unclear. Complicating the task of classifying missense variants in ASD as either pathogenic or benign is that variants associated with polygenic diseases such as ASD are often found in healthy individuals as well, only contributing to disease in combination with other genetic or environmental factors.[57–61] Moreover, the phenotypic spectrum of ASD is so diverse that mild defects often go undiagnosed.[62] Current guidelines for classifying variants recommend using population data only for well-defined Mendelian/monogenic diseases, and functional data obtained in model systems should only be used if well-existing disease mechanisms and many LoF/WT-control variants exist.[63,64] These recommendations fail to provide a framework for classifying variants in a disease such as ASD, which in addition to low-penetrance variants found in both affected and the general population also commonly lacks established molecular mechanisms underlying pathophysiology, disease models, or well-validated, disease-specific functional assays. Here, we contribute to the evolving field of functional variomics,[65–69] which aims to provide comprehensive phenotypic characterization of missense variants, by providing a high-confidence, multi-assay approach toward multifunctional assessment of variant impact. A diversity of functional assays is necessary since proteins are invariably multi-functional and is particularly important when disease-associated molecular mechanisms of pathophysiology are unclear. To address this challenge for the assessment of variants of SYNAGP1, we have developed a panel of assays, including high-throughput multiplex-phospho-flow cytometry and high-content screening, to measure the impact of 57 variants on protein localization, stability, and function in multiple disease-associated signaling pathways, including pERK, pGSK3β, pCREB, and pp38 in human embryonic kidney (HEK293) cells. Since molecular mechanisms associated with ASD are unknown, we present both single-assay functional values, as well as their correlations and a combined multi-functional impact score. Using this novel approach, we find diverse impacts of variants and provide high-confidence functional measures in order to aid clinical classification of variants.

Material And Methods

SYNGAP1 variant selection and cloning

SYNGAP1 Isoform I (GenBank: NM_006772.2) was purchased from Genecopoeia (Genecopoeia, EX-H9502). Variants were selected from a variety of sources, including a database of variants isolated in subjects without serious pediatric disease (gnomAD[70]), the disease-associated variant database ClinVar,[71] the ASD/ID-associated variant databases VariCarta,[72] SFARI,[36] DDD,[73] and MSSNG,[74] as well as clinical literature sources.[2,22,24,30–33,75–81] Variants were generated by three-way Gibson cloning using NEB HiFi DNA Assembly Cloning Kit (NEB, E5520), and a NotI-AscI-digested and purified pENTR backbone (Thermo Scientific, K240020), as well as two PCR-amplified *SYNGAP1* DNA fragments. All variants were then transferred to a custom-made pCAG-mTag-RFP-T-P2A-sfGFP-attr1-ccdb-attr2 destination vector by Gateway cloning (Thermo Scientific, 11791020). Plasmid DNA was isolated using QIAprep Spin Miniprep Kits (QIAGEN, 27106).

Variant assays for stability, function, and localization

We investigated whether different missense variants impact protein stability—a major cause of missense variant dysfunction in other genes.[65,69] To assess this, we used a dual-color mTag-RFP-T-P2A-sfGFP-*SYNGAP1* construct that expresses mTag-RFP-T and sfGFP-tagged SYNGAP1 at equal rates but as two individual proteins. A reduction in GFP/RFP ratio is indicative of protein instability. To determine variant functional impacts, we assayed the phosphorylation states of several signaling proteins within different, synapse-relevant signaling cascades. We selected assays for pERK1/2 and pCREB as promoters of LTP, and pGSK3β and pp38MAPK as promoters of LTD. As previously demonstrated,[56,82] we find that WT GFP-SYNGAP1 localized to discrete cytoplasmic speckles and used CellProfiler to measure the area of speckles for all variants. Individual variant means, error, N, and p values for each assay are provided in Table S2. Complete LoF, partial LoF, and WT-like were defined by variant scores being significantly different from just WT, sfGFP and WT, or just sfGFP, respectively.

Cell culture

HEK293 cells were purchased from the American Type Culture Collection (CRL-1573) and were routinely passaged in Dulbecco's Modified Eagle's Medium (DMEM) (Millipore Sigma D6046) supplemented with 10% FBS and 100 U/mL penicillin-streptomycin (referred to as "culture media" hereafter). For all experiments, HEK293 cells were used for a maximum of 15 passages. For flow cytometry experiments, cells were seeded at 1×10^5 per well in 24-well dishes 16–20 h before transfection with 500 ng of expression plasmid using X-tremeGENE 9 at a ratio of 2 μL to 1 μg DNA. 24 h after transfection, cells were washed with culture media. 24 h later, cells were stimulated for 10 min with fresh culture media, then washed once in 1× PBS before treated with Trypsin-EDTA (GIBCO, 25200072) for 5 min to create a single-cell suspension, and then fixed for 10 min in 3.2% PFA. Cells were then spun down and resuspended in 100% ice-cold methanol, kept at 4°C for 30 min before being moved to −20°C. For high-content imaging, cells

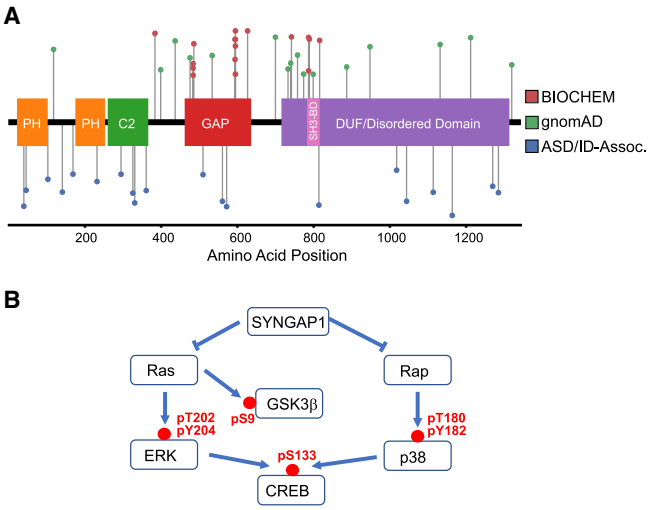

Figure 1. SYNGAP1 variant and functional assay selection
(A) Distribution of variants assayed in this study across the length of SYNGAP1, including known functional domains. Color indicates whether variants were primarily associated with gnomAD, biochemical control (above functional domains), or ASD/ID associated (below functional domains).
(B) Simplified diagram of SYNGAP1 impact on signaling pathways, including phospho-residues assayed in this study.

were seeded at 1.8×10^4 per well in 96-well black-walled collagen-coated plates (Thermo Scientific) 16–20 h before transfection. Cells were fixed in 4% PFA with Hoechst-33342 (1:5,000) for 20 min.

Antibody staining and flow cytometry

Cells were washed with Flow Cytometry Staining Buffer (FC001, R&D Systems) and then incubated in 50 μL of Staining Buffer for 1 h on ice with the following conjugated antibodies multiplexed at the indicated dilutions: (1) mouse monoclonal antibody (mAb) anti-Human pS9-GSK-3β-Alexa Fluor 405, 1:50 (R&D Systems, IC25062V), (2) mouse mAb anti-Human pT202/pY204-pERK1/2-PerCP-eFluor710, 1:200 (Thermo Scientific, 46-9109-41), (3) rabbit mAb anti-Human pT180/pY182-p38MAPK-PE-Cy7, 1:100 (NEB, 51255), (4) rabbit mAb anti-Human pS133-CREB-Alexa Fluor 647, 1:50 (NEB, 14001), (5) mouse mAb anti-Human GAPDH-Dylight680, 1:50 (Thermo Scientific, MA515738D680). Cells were then washed twice with staining buffer before being run on an Attune Nxt Flow Cytometer (Invitrogen). Data were recorded using VL-1 (pGSK3β-Alexa Fluor 405), BL-1 (sfGFP), BL-2 (pERK1/2-PerCP-eFluor710), YL-1 (mTagRFP-T), YL-3 (pp38-PE-Cy7), RL-1 (pCREB-Alexa Fluor 647), and RL-2 (GAPDH-Dylight680) channels, which were single-stain compensated. Using FlowJo, cells were selected using FSC-H/SSC-H and single cells were selected using SSC-H/SSC-A. An in-well untransfected control population was selected using BL-1 (sfGFP) and YL-1 (mTagRFP-T) values within spread of values of untransfected control cells, and a transfected population was selected using BL-1 (sfGFP) values above untransfected to 100-fold above untransfected (Figure S1A).

High-content imaging

Images of 20 fields from each well were collected using the ArrayScan XTI Live High Content Platform (Thermo Scientific). A 20× objective (NA = 0.4, resolution = 0.69 μm) was used to capture widefield images with excitation wavelengths of 386 ± 23, 485 ± 20, and 549 ± 15 nm for imaging of Hoechst, GFP, and RFP, respectively. The emission filter wavelengths are 437 ± 25, 520 ± 12, and 606 ± 23 nm, respectively. CellProfiler 3.0[83] was used to analyze the data by identifying nuclei from Hoechst-positive pixels, to define cytoplasm from RFP signal, and SYNGAP1 expression by GFP signal, respectively. To reduce background noise and imaging artifacts, we applied a filter of nuclei size < 1,000 pixels, cytoplasm size between 500 and 3,000 pixels, and GFP-positive speckle size to between 2 and 3,000 pixels. The size of speckles from a selected set of variants were independently confirmed with high-resolution confocal imaging using a Leica TCS SP5 II Basic VIS confocal system with the researcher blinded to variant identity.

Data analysis

Relative functional values for each reporter-antibody were obtained by the median of (individual transfected cell value – background value) / (in-well untransfected control median value – background value) values normalized to the sfGFP control = 0 and WT SYNGAP1 = 1 except for stability and speckle size, where values were only normalized to WT SYNGAP1 = 1. All data processing, statistical analysis, and clustering was performed in Visual Code using python, matplotlib, sklearn, and seaborn libraries. To calculate individual assay impact scores, absolute functional deviation from WT was calculated by normalizing variant scores to either GFP or the worst-performing variant. Multi-Functional Impact Score was calculated by summing individual assay scores and normalizing to WT's summed score.

Results

ASD/ID-associated missense variants of SYNGAP1 are found throughout the protein

To investigate the impact of variants in multiple domains, we selected 57 variants located throughout the SYNGAP1 protein, including its annotated PH, C2, SH3-binding, and GAP, as well as the C-terminal DUF domains (Figure 1A, Table S1). 23 variants were identified in individuals with ASD/ID and were assigned the primary category ASD/ID associated. Individual variants associated with ASD occurring in multiple probands are exceedingly rare, and due to low penetrance of any single allele and the nature of the wide spectrum of phenotypes associated with ASD, are often found in the general population as well; we thus considered variants ASD/ID associated as long as they were identified in at least one individual with these disorders. This relatively nonbiased approach to categorization of variants in this study should not be taken as a presumption of pathogenicity. We also included a set of 17 likely loss-of-function (LoF) or gain-of-function (GoF) variants, termed biochemical controls (BIOCHEM), which are mutations at known phosphorylation target sites of kinases that regulate SYNGAP1 catalytic ability (CaMK2: Ser1165; CDK5: Ser788, Thr790, Ser817; PLK2: Ser385), as well as variants at sites described as LoF in non-human orthologs of SYNGAP1 (Arg485, Asn487, Leu595, and Arg596).[2,22,24,81] A total of 16

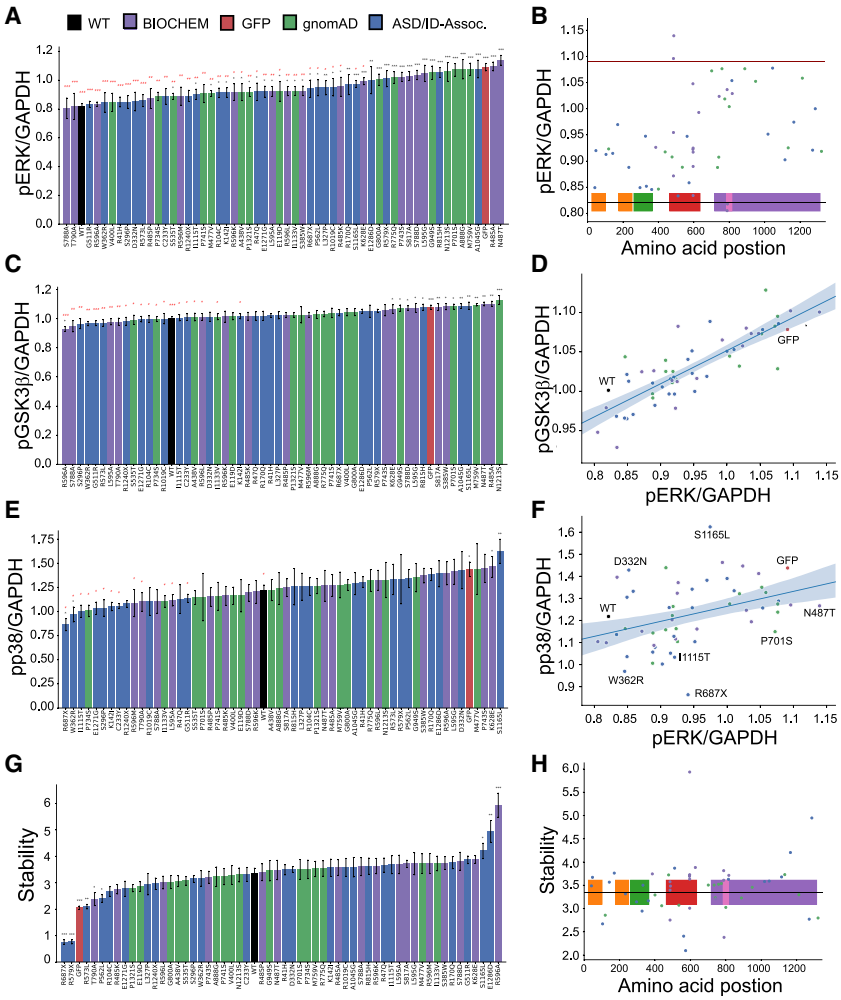

Figure 2. Functional differences of SYNGAP1 variants in ERK, GSK3β, p38 signaling, and stability

(A) Relative pERK/GAPDH value of transfected cells/untransfected cells. Median value of each well averaged across wells, n ≥ 4 wells for all variants. Color indicates primary variant association.

(B) Distribution of pERK functional scores across the length of SYNGAP1, including domains overlaid at bottom. Red line indicates GFP level, black line indicates WT SYNGAP1.

(C) Relative pGSK3β/GAPDH value of transfected cells/untransfected cells. n ≥ 4 for all variants.

(D) Scatterplot of pERK versus pGSK3β functional scores with linear regression. Pearson r = 0.83, p = 4.7×10^{-15}.

(E) Relative pp38/GAPDH value of transfected cells/untransfected cells. Median value of each well averaged across wells, n ≥ 4 wells for all variants.

(F) Protein stability functional value as GFP/RFP ratio of transfected cells. Median value of each well averaged across wells, n ≥ 4 wells for all variants.

(G) Scatterplot of pERK versus pp38 functional scores with linear regression with select variants with largest differences between the two measures highlighted. Pearson r = 0.36, p = 0.006.

(H) Distribution of stability scores across the length of SYNGAP1, including domains overlaid at bottom. Black line indicates WT SYNGAP1.

For all panels, *p < 0.05, **p < 0.005, ***p < 0.001 to WT and # p < 0.05, ## p < 0.005, ### p < 0.001 to GFP by t test. All error bars are standard error of the mean (SEM). For (D) and (F), shaded area around the regression line indicates the standard error of the estimate.

variants have not been identified in any patients to date but were found in a database of people without reported pediatric disease (gnomAD[70]). Detailed annotation, population frequencies, and sourcing of all variants tested can be found in Table S1. Variants selected were located across the length of the protein, including the four well-annotated domains, 2xPH, C2, and the Ras/Rap-GAP domain, and within a disordered domain of unknown function (DUF).

SYNGAP1 missense variants exhibit deficits in inhibiting ERK and GSK3β phosphorylation

To study the effects of missense mutations on multiple functions of SYNGAP1, we assayed phosphorylated residues of signaling proteins directly downstream of known SYNGAP1 function (Figure 1B). We measured SYNGAP1-mediated Ras-signaling by assaying phosphorylation states of ERK (pT202/pY204), which is located within the canonical MAPK cascade downstream of Ras,[3,44,47,50] as well as both pS9 on GSK3β and pS133 on CREB, which are known to be indirectly regulated by Ras.[48,52,55,84] To assess SYNGAP1 function toward Rap, we assayed pT180/pY182 on p38 MAPK, which is known to be regulated by SYNGAP1 via MUPP1.[13,23,50]

We first measured the level of phosphorylated ERK1/2, which correlates with Ras activation and is downregulated by SYNGAP1 (Figure 1B). WT SYNGAP1 reduced phosphorylation of ERK1/2 by 28% compared to levels in untransfected cells. We found that variants exhibited a wide range of dysfunction, with 18/57 variants showing complete LoF and 22/57 demonstrating partial LoF (Figure 2A). The two missense variants with the lowest (p.Arg485Ala [c.1453C>G + 1454G>C] and p.Asn487Thr [c.1460A>C]) and highest (p.Ser788Ala [c.2362T>G] and p.Thr790Ala [c.2368A>G]) functional scores were biochemical controls located in the RasGAP and SH3-binding domain, respectively. p.Arg485Ala and p.Asn487Thr have been previously described as LoF variants in RasGAPs, while p.Ser788Ala is a known gain-of-function (GoF) variant and p.Thr790Ala is hypothesized to be a GoF variant based on its proximity to Ser788.[2,5,81] Notably, we observed that across variants, dysfunction was more severe in C-terminal variants, with no variant exhibiting less than 50% function located before aa 485 and all variants

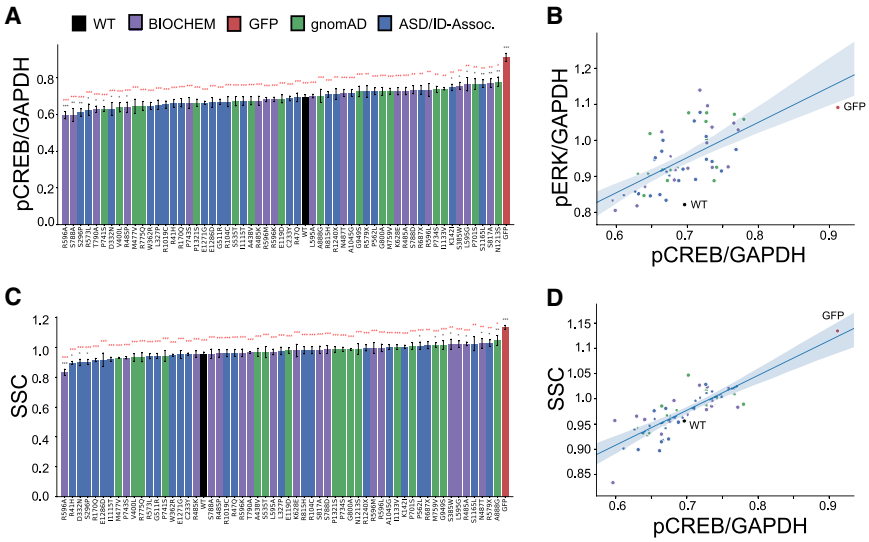

Figure 3. Functional differences of SYNGAP1 variants in CREB signaling and SSC scores

(A) Relative pCREB/GAPDH value of transfected cells/untransfected cells. Median value of each well averaged across wells, $n \geq 4$ wells for all variants. Color indicates primary variant association.

(B) Scatterplot of pCREB versus pERK functional scores with linear regression. Pearson $r = 0.62$, $p = 3.4 \times 10^{-7}$.

(C) Relative SSC value of transfected cells/untransfected cells. $n \geq 4$ for all variants.

(D) Scatterplot of pCREB versus SSC functional scores with linear regression. Pearson $r = 0.77$, $p = 6.3 \times 10^{-12}$.

For all panels, *$p < 0.05$, **$p < 0.005$, ***$p < 0.001$ to WT and # $p < 0.05$, ## $p < 0.005$, ### $p < 0.001$ to GFP by t test. All error bars are standard error of the mean (SEM). For (B) and (D), shaded area around the regression line indicates the standard error of the estimate.

past aa 800 exhibiting significant LoF (Figure 2B). In particular, two variants in the C-tail, p.Ala1045Gly (c.3134C>G) and p.Asn1213Ser (c.3638A>G), exhibited prominent LoF. We find variants located in well-annotated structural domains such as the two PH domains, the C2 domain, and the GAP domain to generally have less severe of an impact than variants within the DUF domain that makes up the latter half of the protein. Interestingly, our results revealed two variants, p.Pro701Ser (c.2101C>T) and p.Met759Val (c.2275A>G), located in the uncharacterized region between the RasGAP and the SH3 binding domains, which exhibited severe LoF not previously reported.

Inhibitory effects of SYNGAP1 on the Ras/ERK pathway have been widely described.[4,8,39,47,50] Here, we demonstrate for the first time that SYNGAP1 also regulates a parallel Ras/GSK3β pathway. Overexpression of WT SYNGAP1 leads to dephosphorylation at Ser9, and thus activation of GSK3β[52] (Figure 2C). Importantly, the degree of dysfunction of SYNGAP1 variants with respect to ERK inhibition highly correlated with the amount of GSK3β activation, but with lower magnitude (Figure 2D).

p38MAPK is known to be a downstream target of SYNGAP1 (Figure 1B), and we find that WT SYNGAP1 overexpression significantly dephosphorylates p38 MAPK.[13,23] However, few of the SYNGAP1 variants showed significant difference compared to WT (Figure 2E), such as LoF of the ASD-associated variant and biochemical control p.Ser1165Leu (c.3494C>T), which is known to link SYNGAP1 activity to p38 via CAMK2.[2] Comparing functional scores of variants in markers associated with LTP (pERK) and LTD (pp38), we find that while the overall correlation of SYNGAP1 variant impact is strong (Figure 2F), we identify both variants with much higher function toward pERK than pp38 (p.Asp332Asn [c.994G>A] and p.Ser1165Leu), and variants with the opposite phenotype of much lower function toward pp38 than pERK (p.Trp362Arg [c.T1084A>C], p.Ile1115Thr [c.3344T>C], p.Arg687Stop [c.2059C>T], p.Pro701Ser, and p.Asn487Thr). Determining the impact of these variants on neuronal synaptic plasticity assays is warranted.

Missense-induced protein instability is not a major cause of dysfunction in SYNGAP1

We next explored whether protein instability contributes to observed LoF, since instability is a major mechanism of missense variant dysfunction for other proteins.[65,69,85,86] However, we find SYNGAP1 to be largely resistant to missense-induced instability, with only 3 of the 57 missense variants tested, p.Arg573Leu (c.1718G>T), p.Thr790Ala, and p.Pro562Leu (c.1685C>T), exhibiting significant loss of stability (Figure 2G). The two early termination variants p.Arg579Stop (c.1735C>T) and p.Arg687Stop were, unsurprisingly, the most unstable, showing ~23% of WT protein abundance. p.Arg1240Stop (c.3718C>T), however, despite missing the last ~100 aa of the protein, retained 88% of WT stability. Three missense variants showed significant hyper-stability (p.Ser1165Leu, p.Glu1286Asp [c.3858A>T], and p.Arg596Ala [c.1786C>G + 1787G>C]), and in the case of p.Arg596Ala, the increase of ~80% was dramatic. We find strong effects of variants on protein stability largely restricted to a small part of SYNGAP1's GAP domain and the C terminus (Figure 2H).

Dephosphorylation of CREB independent of ERK/GSK3β dysfunction

The transcription factor CREB is a major regulator of neuronal plasticity and survival and is downstream of several disease-associated signaling pathways, including Ras-ERK[87,88] (Figure 1B). We find that WT SYNGAP1 significantly decreases levels of pCREB by 26%, similar to its effects on pERK. Moreover, we find that while some variants were fully unable to inhibit ERK, all variants tested suppressed CREB phosphorylation (Figure 3A). 8/57 variants

exhibited partial LoF, including known LoF variants at sites phosphorylated by CDK5 (p.Ser817Ala [c.2449T>G]) and CAMK2 (p.Ser1165Leu), while 9/57 variants had a GoF phenotype, including the known GoF variants p.Ser788Ala and p.Thr790Ala. While functional scores for pCREB were correlated to pERK functional scores (Figure 3B), they were more strongly correlated with the flow-cytometry physical property readout side scatter (SSC), a measure of cell granularity (Figures 3C and 3D). Changes in SSC are associated with apoptosis and cell death, which is regulated by pCREB levels in neurons.[87,89–91]

SYNGAP1 variants exhibit altered subcellular localization

In neurons, SYNGAP1 localizes to subcellular speckle domains associated with the PSD.[6,14] To further characterize the functional impact of variants, we examined their subcellular localization when expressed in HEK293 cells. WT SYNGAP1 localizes to cytoplasmic speckles (Figure 4A), a phenotype that has been previously observed in cell lines.[56,82] Further, naturally occurring truncated C-terminal isoforms and select C-terminal missense variants (p.Leu1202Asp [c.3605A>G + 3606T>A] and p.Lys1252Asp [c.3754C>G + 3756GA>T]) prevent SYNGAP1 co-localization with PSD95 in subcellular speckles in neurons.[82,92] More than half (45/57) of SYNGAP1 variants assayed here showed a significant increase in mean speckle area (Figure 4B). Seven variants had a much larger increase in mean speckle area, including the two early termination variants p.Arg687Stop and p.Arg579Stop, the two unstable missense variants p.Pro562Leu and p.Arg573Leu, and three variants close to, or within, the C2 domain (p.Leu327Pro [c.980T>C], p.Cys233Tyr [c.698G>A], and p.Trp362Arg; Figure 4C). All seven of these variants are ASD/ID associated. Four variants, including the C-terminal missense variant p.Glu1286Asp and a variant lacking the C-terminal domain altogether (p.Arg1240Stop), exhibited a phenotype of having smaller speckles. Notably, no variant assayed in this study exhibited an absence of speckles and diffuse cytoplasmic distribution. After removal of outlier variants (>3*Interquartile Range (IQR) away from 25%/75% quartiles) from correlation analyses, we detect significant correlation between our functional pCREB/GAPDH score and speckle area—variants with larger speckles had larger LoF in our pCREB assay (Figure 4D)—providing a link between functional and localization scores.

Clustering analyses

Normalized functional scores for all variants across measures are shown in Figure 5A. Overall, we find strong correlation of functional scores across different signaling assays, but not between signaling and localization assays, with the exception of significant negative correlation between speckle area and CREB phosphorylation (Figures 5B and S1B). We applied two approaches toward clustering analysis. First, we clustered variants by functional measure scores generating a cluster heatmap to highlight the most closely correlated variants (Figure 5C). Notably, p.Arg596Ala is not closely correlated to any other variant in the study, likely because of its strong GoF phenotype in stability and across signaling assays. Cluster results reveal that missense variants distributed across SYNGAP1 can have very similar effects on a wide range of phenotypes, such as p.Arg485Ala and p.Met759Val, or p.Ile1133Val (c.3397A>G) and p.Lys142Ile (c.425A>T), the two most similar pairs of variants in this study.

Second, to illustrate large-scale associations and clusters of variants, we performed principal component analysis (PCA) followed by KMeans clustering on the entire dataset (Figures 5D and S1C). The first PC axis (PC-1) accounts for 44.9% of variation in the dataset and is largely made up of phospho-flow scores, while the second PC axis (PC-2) features mostly stability and speckle phenotypes, accounting for 27.3% of variation. KMeans clustering reveals five groups of variants: a set of variants that are largely LoF across phenotypes (blue), a second set of variants that are largely WT-like across phenotypes (black), as well as three additional clusters containing variants with outlier phenotypes in a subset of assays. The two nonsense variants p.Arg687Stop and p.Arg579Stop as well as the missense variant p.Pro562Leu are part of the first outlier cluster (yellow) as three of the only five variants in this study that exhibited protein instability. The fourth and fifth clusters contain many GoF variants. While the fourth cluster (red) mainly contains variants with catalytic GoF phenotypes and larger speckles, the fifth cluster (green) contains the two hyper-stable variants, p.Glu1286Asp and p.Arg596Ala, which also have smaller speckles.

Multi-parametric functional impact scoring

To provide an overall score for each variant, we first normalized individual assay functional results to either GFP, where GFP appropriately described complete LoF (pERK, pGSK3β, and pp38), or to the worst-performing variant (pCREB, SSC, stability, and speckle area), as well as to WT. GoF was treated the same as LoF as we scored a variant's absolute deviation in function from WT. We then summed individual assay results with equal weights and normalized to WT's multi-functional score sum to provide a multi-functional impact score between 0 (no function) and 1 (WT-like function, Figure 6A). We find variants exhibiting a range of multi-functional impact scores throughout the protein (Figure 6B), as well as in all three categories of annotation: variants associated with ASD/ID, variants found in the healthy population (gnomAD), and biochemical controls (Figure 6C). We propose that in particular gnomAD variants with high functional scores such as p.Ala438Val (c.1313C>T), p.Glu119Asp (c.357G>T/C), and p.Pro1321Ser (c.3961C>T) should be used as WT-like, functionally normal controls, and ASD-associated and biochemical controls at positions throughout the

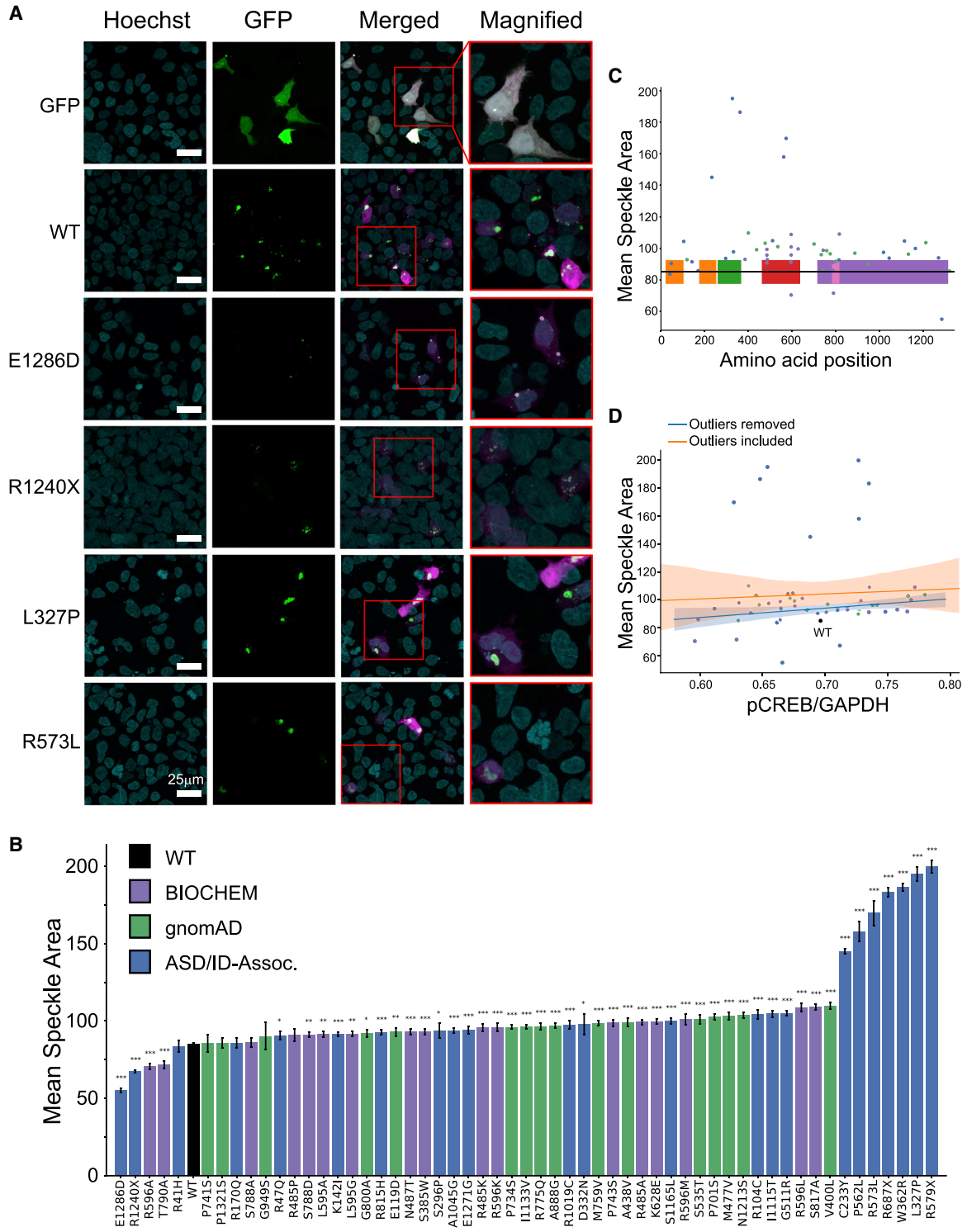

Figure 4. Variants of SYNGAP1 exhibit altered subcellular speckle localization

(A) Representative confocal images showing subcellular localization of GFP, GFP-SYNGAP1 WT and selected variants with smaller (p.Glu1286Asp, p.Arg1240Stop) and larger (p.Leu327Pro, p.Arg573Leu) mean speckle size than WT in HEK293 cells. Cell nuclei were stained with Hoechst (cyan), GFP signal in green, RFP transfection signal in magenta. Scale bar 25 μm.

(B) Distribution of variant functional scores for mean speckle area measured pixel size of GFP-SYNGAP1 speckle. Mean value of all speckles within transfected cells that passed quality filter (see material and methods) taken from all wells. n ≥ 11 wells for all variants. *p < 0.05 compared to WT. Error bars are standard error of the mean (SEM).

(C) Distribution of mean speckle area scores across the length of SYNGAP1, including domains overlaid at bottom. Black line indicates WT SYNGAP1.

(D) Scatterplot of pCREB versus nuclear localization functional scores with linear regression with (orange) and without (blue) outlier variants included. Pearson r = 0.3, p = 0.01 for regression after outlier removal. Shaded area around the regression line indicates the standard error of the estimate.

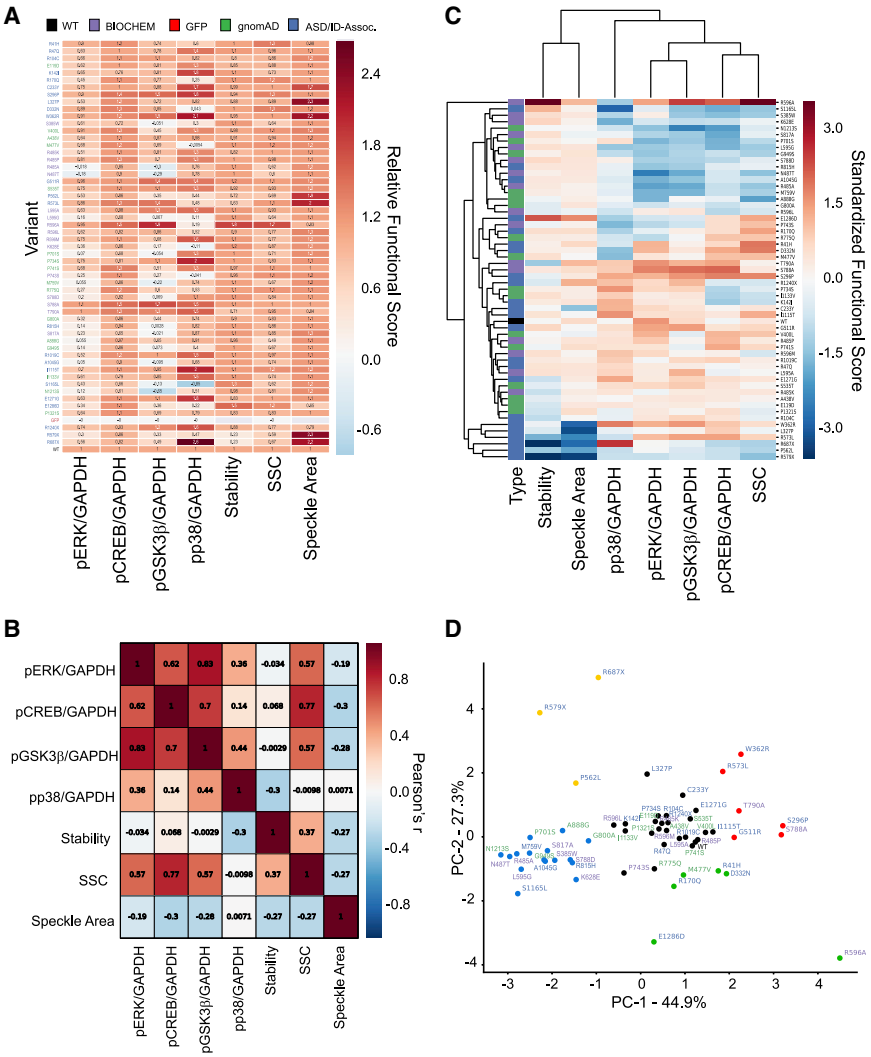

Figure 5. Clustering of SYNGAP1 variants by multi-parameter functional assay scores

(A) Heatmap of all variant functional scores across assays normalized to WT = 1 and GFP = 0 except for nuclear localization and stability. Variants are ordered by amino acid position, with early termination variants, GFP, and WT at the bottom.

(B) Correlation matrix of Pearson r values.

(C) Hierarchical clustering heatmap of variants and assays calculated from standardized functional scores using Seaborn library. Blue-red gradient indicates standardized variant score in respective assay.

(D) KMeans clustering after PCA performed on all variants in the study. PC-1 accounts for 44.9% of variation in the data, PC-2 accounts for 27.3%. PC-1 primarily accounts for signaling functional scores PC-2 primarily accounts for localization and stability phenotypes (see Figure S1C for PC axis weights).

protein with very low functional scores such as p.Ser1165Leu, p.Arg596Ala, p.Leu595Gly (c 1783C>G + 1784T>G), p.Glu1286Asp, and p.Arg485Ala should be used as LoF, functionally abnormal controls in future studies, particularly with neuronal measures, to elucidate *SYNGAP1*'s role in pathogenesis.

Of the 57 variants assayed in this study, 20 had existing ClinVar clinical pathogenicity annotations as either likely benign/benign (LB/B), VUS/conflicting (CONF), or likely pathogenic/pathogenic (LP/P). Based on our seven assays, we are able to compare existing ClinVar annotations to our high-confidence multi-functional impact scores (Figure 6D). Nine variants in ClinVar are annotated as LP/P, including three of the four lowest-scoring variants in our study (p.Arg579Stop, p.Arg687Stop, and p.Ser1165Leu). We find a range of dysfunction across all scored and unscored variants, indicating the need for additional and more nuanced clinical annotation of variants, well-founded variant pathogenicity predictions, and efforts directed toward linking molecular dysfunction and functional assays to disease states.

Discussion

We have characterized the functional effects of 57 variants of SYNGAP1 in seven different functional assays. While the impact of biochemical control variants on ERK inhibition is consistent with previous findings,[4,8] our results discriminate effects of mutations in different domains specific to distinct functions of SYNGAP1, allowing high-confidence functional impact metrics for establishing variant pathogenicity prediction. We find a range of functionality from complete LoF, partial LoF, fully WT-like, to GoF on the impact of SYNGAP1 variant overexpression on pERK and pGSK3β, while all variants assayed retained at least partial function to downregulate pCREB. These results indicate that the inhibitory effects of SYNGAP1 on CREB are not solely due to its action on Ras/ERK/GSK3β. We also find variants with large differences in their ability to dephosphorylate downstream reporters of Ras/Rap activity, suggesting they may show distinct effects on SYNGAP1-mediated LTP/LTD balance.[9,10,82]

We find that variants affect the ability of SYNGAP1 to localize to cytoplasmic speckles, providing support for dysregulation of localization in pathogenesis. Interestingly, variants that exhibited a reduction in mean speckle size were better able to dephosphorylate CREB. While CREB is primarily localized in the nucleus in both neurons and HEK293 cells,[93] our results indicate that CREB dephosphorylation by SYNGAP1 may take place in the cytoplasm. In neurons, phosphorylated CREB is also found in axons and dendrites, and regulation of CREB phosphorylation plays an important role in neuronal survival, synaptic

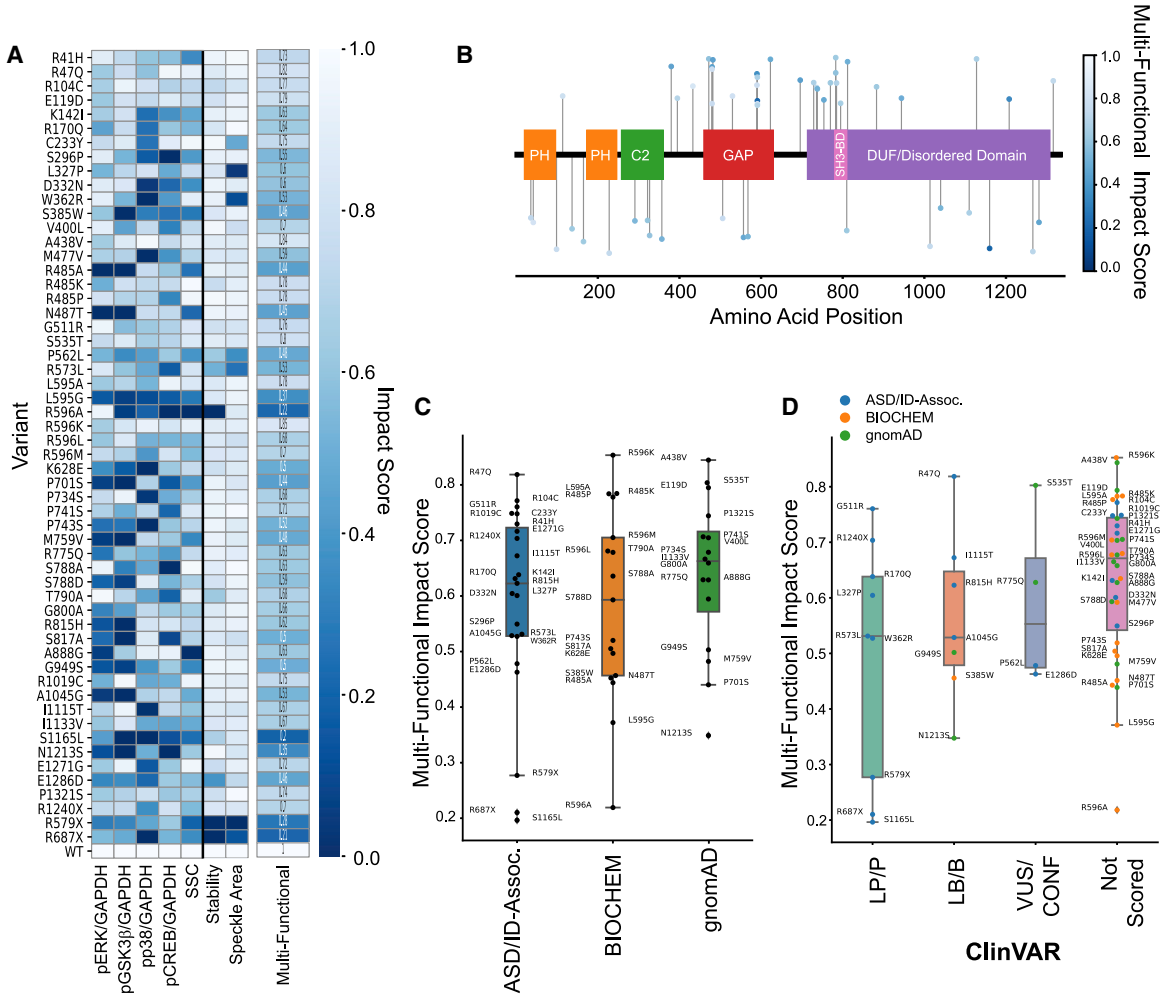

Figure 6. High confidence, multi-functional impact scores of SYNGAP1 variants

(A) Individual assay functional impact scores obtaining by normalizing variants to WT and either GFP (pERK/GAPDH, pGSK3β/GAPDH, and pp38/GAPDH) or worst-performing variant (pCREB/GAPDH, SSC, stability, and speckle area), as well as multi-functional impact score calculated as sum of individual assays normalized to WT value of 1. Darker color indicates lower functional score.

(B) Distribution of multi-functional impact scores across the length of SYNGAP1, including domains overlaid. ASD/ID-associated variants plotted below, non-ASD/ID-associated variants above.

(C) Multi-functional impact score distribution of variants associated with either ASD/ID, gnomAD, or biochemical variants. Boxplot indicates median and IQR. Whiskers note all non-outliers points within IQR*1.5 range.

(D) Multi-functional impact score distributions of variants with existing ClinVar annotation (LP/P, LB/B, or VUS/CONF) as well as variants that have not yet been scored. Association of variants with either ASD/ID, gnomAD, or biochemical variants indicated by color of data point.

plasticity, and dendritic growth.[94–99] Supporting our findings of some C2-domain variants exhibiting localization to significantly larger speckles, C2 domains in other proteins are known to bind to phospholipids at the plasma membrane, and missense mutations in the C2 domain cause mislocalization.[100–104] Surprisingly, variants localized within the disordered DUF domain in the C-terminal half of the protein exhibited the most significant dysfunction in our signaling assays, to a greater extent than variants within the GAP domain. These results support further characterization of the DUF domain and its interaction with SYNGAP1's GAP domain for understanding missense variant-induced SYNGAP1 dysfunction.[105–107] Our multiplex platform also identifies LoF variants outside of annotated domains such as two variants located between the SH3-binding and GAP domains (p.Pro701Ser and p.Met759Val).

We hypothesize that few of the variants in our study contribute to protein instability presumably because as a 1,343 aa protein, SYNGAP1 is relatively large and can compensate for individual aa substitutions. Indeed, a multi-protein comparative study analyzing missense variants has confirmed the trend that larger proteins tend to be more resistant to missense-induced instability.[108] Two of the three instability-inducing variants we identified are located within a span of 11 aa in the center of the GAP domain contributing to a short α5c-helix identified in SYNGAP1's crystal structure.[5,81] Further, one of the

three unstable variant, p.Pro562Leu, has previously been found to be unstable.[5,32] These results indicate that only mutations in discrete regions of SYNGAP1 may induce instability. We find two variants that exhibited significant GoF phenotypes across several assays. One of these variants, p.Arg596Ala, is localized in a highly conserved GAP motif, an FLR arginine-finger loop that determines substrate specificity across RasGAPs.[81] Since an alanine substitution of Arg596 is expected to disrupt this motif, it is surprising that p.Arg596Ala both significantly increases protein stability and retains or enhances function. Interestingly, other substitutions at the same site to either lysine, methionine, or leucine had either a much weaker or no effect. Since two of the three missense variants with instability were located close to this residue (p.Arg573Leu and p.Pro562Leu), it is possible that the molecular mechanisms underlying their instability and p.Arg596Ala's hyper-stability are linked. Further study of the FLR loop in SYNGAP1 and how it differs from other RasGAPs such as p120GAP and NF-1 is warranted. Another GoF variant, p.Glu1286Asp, on the other hand, is a seemingly minor change from one negatively charged residue to another. While deleterious effects of this conservative substitution have been described in functional roles and thermal stability, it is not well characterized.[109,110] The effect of C-terminal substitutions on SYNGAP1 localization in our assay is similar to results from removing the last 100 aa of SYNGAP1. p.Arg1240Stop exhibits a GoF phenotype similar to p.Glu1286Asp, and both of these variants localize to aberrant, smaller cytoplasmic speckles. The function of the C-terminal domain of SYNGAP1, specifically the α2-isoform used in this study, remains elusive. Our results indicate that the C-terminal domain of SYNGAP1-α2 regulates subcellular localization, a critical role of SYNGAP1 in neurons.[82,92] Despite lacking the C-terminal QTRV-motif found in the α1 isoform, which confers binding to PDZ motifs and activity-dependent movement from the PSD core,[29,111] α2 is similarly able to localize to the PSD in neurons.[15]

We find that the biochemical control and ASD/ID-associated variant p.Ser1165Leu exhibited more LoF than the two early termination variants p.Arg579Stop and p.Arg687Stop and would advocate it be included as a functionally abnormal LoF control in future studies. Similarly, the two FLR-loop variants p.Leu595Gly and p.Arg596Ala had very low multi-functional impact scores—but for distinct reasons: p.Leu595Gly exhibited severe LoF across assays, while p.Arg596Ala showed severe GoF. Interestingly, three different substitutions at the same sites (p.Arg596Lys [c.1786C>A+1787G>A], p.Arg596Met [c.1786C>A+1787G>T], and p.Leu595Ala [c.1783C>G,1784T>C]) were generally WT-like, indicating that only specific aa changes may have severe impacts at these sites. Similarly, biochemical controls derived from RasGAP-conserved domains had different effects based on the type of aa substitution. While p.Arg485Ala exhibited LoF with a low multi-functional impact score, both p.Arg485Lys (c.1453C>A + 1454G>A) and p.Arg485Pro (c.1454G>C) showed WT-like function.

Our results of variant impact on multiple SYNGAP1 protein functions allows correlation with existing annotations. Unfortunately, for the majority of SYNGAP1 variants, current classifications have often been based solely on bioinformatic tools predicting impact on protein function, or assumptions based on frequency of occurrence in the general population. Bioinformatics predictive tools are largely untested and are not gene specific, resulting in mixed correlation to empirical measures.[65,112,113] Variant frequency in the population should be used with caution in predicting association with ASD since common variants may contribute to this disorder under specific genetic backgrounds or environments.[58,60–63] Comparing existing ClinVar pathogenicity predictions to our multi-functional impact scores, two variants in the LP/P category exhibited noticeably high function: p.Gly511Arg (c.1531G>C) and p.Arg1240Stop. p.Gly511Arg is present in ClinVar as a single LP submission with no condition information and was identified in one individual with epilepsy and autism. Notably, the p.Gly511Arg substitution (exons 5/6 −1 G>A) and a second LP/P variant, p.Arg170Gln (exons 9/10 −1 G>A), are caused by genomic changes located in close proximity to intron/exon boundaries. While the aa substitution might be benign, it is possible that the change in nucleotide sequence affects splicing to induce a much more severe disruption of SYNGAP1 structure and function, which our assays of cDNA changes are incapable of detecting. p.Arg1240Stop, on the other hand, is a variant lacking the C-terminal tail shown to be essential for the association of SYNGAP1 with PSD95,[29,82] a phenotype likely critical for neuronal synaptic functions not assessed by our HEK293 assays.

Seven missense variants of SYNGAP1 assayed in this study are present in ClinVar and annotated as LB/B: p.Arg47Gln (c.140G>A), p.Ser385Trp (c.1154C>G), p.Arg815His (c.2444G>A), p.Gly949Ser (c.2845G>A), p.Ala1045Gly, p.Ile1115Thr, and p.Asn1213Ser. While our results show p.Arg47Gln, and to a lesser extent p.Ile1115Thr, exhibited high multi-functional scores, the other variants in this category showed a surprising amount of dysfunction. p.Ser385Trp is a biochemical control and Ser385 is a confirmed target for PLK2.[22,24] p.Ala1045Gly is one of the most common SYNGAP1 variants in gnomAD and was classified as benign due to this high frequency.[70] However, both p.Ala1045Gly and p.Arg815His exhibit complete LoF for both pERK and pGSK3β inhibition in our assays and have also been identified in an individual with ASD/ID.[76,79] To date, p.Asn1213Ser and p.Gly949Ser have not been reported in individuals affected by ASD/ID and p.Asn1213Ser is located close to one of SYNGAP1's trimer-interfaces[92] —both variants are complete LoF in our pERK and pGSK3β assays. While our multi-faceted functional assays may not be fully representative of disease-associated pathophysiology, these findings highlight that for

low-penetrance variants in polygenic diseases, ClinVar annotations, particularly LB/B, require additional evidence, and the heightened presence of an allele in the general population does not necessarily indicate that an allele has no loss of function. Indeed, large-scale sequencing studies find the presence of seemingly deleterious alleles in otherwise healthy populations at frequencies of more than 100 LoF variants per person.[114,115] Further, other genes in similar polygenic diseases, such as hypertrophic myocardiopathy, exhibit high-frequency, low-penetrance pathogenic alleles.[57]

This hurdle for predicting variant pathogenicity is even higher for polygenic disorders with large numbers of rare single-nucleotide variants such as ASD, where most variants are only ever identified in a single proband and disease phenotypes are complex. In order to address these issues for SYNGAP1, here we have developed a pipeline to asses multiple independent and correlated functions of SYNGAP1 to provide high-confidence individual assay and combined, multi-functional impact scores to guide pathogenicity prediction. We provide high (p.Ser535Thr [c.1604G>C]) and low (p.Pro562Leu and p.Glu1286Asp) multi-functional impact scores as strong evidence for classification of three of the four variants in ClinVar currently annotated as VUS/CONF. Further, our findings will aid in annotation of ASD/ID-associated variants that have not yet been scored, particularly those we find to exhibit high multi-functional scores such as p.Arg104Cys (c.310C>T), or low multi-functional scores such as p.Met759Val. Our study also highlights variants with mixed results which would benefit from additional study, particularly in neuronal models, to assess their potential contributions to disease in more detail. We define multiple disease-associated and biochemical variants with well-validated, multiple-assay LoF or WT-like effects to serve as functionally normal and functionally abnormal controls in future studies of SYNGAP1. Since additional, novel variants of SYNGAP1 are constantly identified in probands, our scalable high-throughput framework combined with validated controls allows rapid and comprehensive assessment of the functionality of SYNGAP1 variants in the future. Moreover, for any variant of any gene where the molecular link to disease is not well defined, this framework can serve as a means to integrate results from multiple independent assays into a combined, multi-functional impact score to aid in pathogenicity predictions.

Data and code availability

No additional datasets or code are associated with this paper. All flow cytometry data were analyzed using FlowJo software, and high-content imaging was analyzed using CellProfiler 3.0. This work makes use of the following publicly available databases: gnomAD v2.1.1, ClinVar, VariCarta1, SFARI Gene, ExAC, MSSNG, and SCHEMA.

Supplemental Data

Supplemental Data can be found online at https://doi.org/10.1016/j.ajhg.2020.11.011.

Acknowledgments

This work was supported by a grant from the Simons Foundation/SFARI (Grant #573845, Grantees K.H. and P.P.) and a CIHR Foundation Award (K.H.). We would like to acknowledge Manuel Belmadani, Eric Chu, and Nathan Holmes for their assistance on variant selection and annotation.

Declaration of interests

The authors declare no competing interests.

Received: April 16, 2020
Accepted: November 16, 2020
Published: December 11, 2020

Web resources

CellProfiler 3.0, https://cellprofiler.org/
ClinVar, https://www.ncbi.nlm.nih.gov/clinvar/
ExAC, http://exac.broadinstitute.org/
FlowJo, https://www.flowjo.com/
GenBank, https://www.ncbi.nlm.nih.gov/genbank/
gnomAD v2.1.1, https://gnomad.broadinstitute.org/
MSSNG, https://research.mss.ng/
OMIM, https://www.omim.org/
SCHEMA, https://schema.broadinstitute.org/
SFARI Gene, https://gene.sfari.org/
VariCarta1, https://varicarta.msl.ubc.ca

References

1. Jeyabalan, N., and Clement, J.P. (2016). SYNGAP1: Mind the Gap. Front. Cell. Neurosci. *10*, 32.
2. Walkup, W.G., 4th, Washburn, L., Sweredoski, M.J., Carlisle, H.J., Graham, R.L., Hess, S., and Kennedy, M.B. (2015). Phosphorylation of synaptic GTPase-activating protein (synGAP) by Ca2+/calmodulin-dependent protein kinase II (CaMKII) and cyclin-dependent kinase 5 (CDK5) alters the ratio of its GAP activity toward Ras and Rap GTPases. J. Biol. Chem. *290*, 4908–4927.
3. Araki, Y., Zeng, M., Zhang, M., and Huganir, R.L. (2015). Rapid dispersion of SynGAP from synaptic spines triggers AMPA receptor insertion and spine enlargement during LTP. Neuron *85*, 173–189.
4. Wang, C.C., Held, R.G., and Hall, B.J. (2013). SynGAP regulates protein synthesis and homeostatic synaptic plasticity in developing cortical networks. PLoS ONE *8*, e83941.
5. Pena, V., Hothorn, M., Eberth, A., Kaschau, N., Parret, A., Gremer, L., Bonneau, F., Ahmadian, M.R., and Scheffzek, K. (2008). The C2 domain of SynGAP is essential for stimulation of the Rap GTPase reaction. EMBO Rep. *9*, 350–355.
6. Kim, J.H., Liao, D., Lau, L.F., and Huganir, R.L. (1998). SynGAP: a synaptic RasGAP that associates with the PSD-95/SAP90 protein family. Neuron *20*, 683–691.

7. Chen, H.J., Rojas-Soto, M., Oguni, A., and Kennedy, M.B. (1998). A synaptic Ras-GTPase activating protein (p135 SynGAP) inhibited by CaM kinase II. Neuron *20*, 895–904.
8. Gamache, T.R., Araki, Y., and Huganir, R.L. (2020). Twenty years of syngap research: From synapses to cognition. J. Neurosci. *40*, 1596–1605.
9. Nicoll, R.A. (2017). A Brief History of Long-Term Potentiation. Neuron *93*, 281–290.
10. Herring, B.E., and Nicoll, R.A. (2016). Long-Term Potentiation: From CaMKII to AMPA Receptor Trafficking. Annu. Rev. Physiol. *78*, 351–365.
11. Zhang, L., Zhang, P., Wang, G., Zhang, H., Zhang, Y., Yu, Y., Zhang, M., Xiao, J., Crespo, P., Hell, J.W., et al. (2018). Ras and Rap Signal Bidirectional Synaptic Plasticity via Distinct Subcellular Microdomains. Neuron *98*, 783–800.e4.
12. Zhu, J.J., Qin, Y., Zhao, M., Van Aelst, L., and Malinow, R. (2002). Ras and Rap control AMPA receptor trafficking during synaptic plasticity. Cell *110*, 443–455.
13. Krapivinsky, G., Medina, I., Krapivinsky, L., Gapon, S., and Clapham, D.E. (2004). SynGAP-MUPP1-CaMKII synaptic complexes regulate p38 MAP kinase activity and NMDA receptor-dependent synaptic AMPA receptor potentiation. Neuron *43*, 563–574.
14. Yang, Y., Tao-Cheng, J.H., Reese, T.S., and Dosemeci, A. (2011). SynGAP moves out of the core of the postsynaptic density upon depolarization. Neuroscience *192*, 132–139.
15. Yang, Y., Tao-Cheng, J.H., Bayer, K.U., Reese, T.S., and Dosemeci, A. (2013). Camkii-Mediated Phosphorylation Regulates Distributions of Syngap-α1 and -α2 at the Postsynaptic Density. PLoS ONE *8*, e71795.
16. Fu, Z., Lee, S.H., Simonetta, A., Hansen, J., Sheng, M., and Pak, D.T.S. (2007). Differential roles of Rap1 and Rap2 small GTPases in neurite retraction and synapse elimination in hippocampal spiny neurons. J. Neurochem. *100*, 118–131.
17. Finkbeiner, S., and Greenberg, M.E. (1996). Ca(2+)-dependent routes to Ras: mechanisms for neuronal survival, differentiation, and plasticity? Neuron *16*, 233–236.
18. Panayotis, N., Karpova, A., Kreutz, M.R., and Fainzilber, M. (2015). Macromolecular transport in synapse to nucleus communication. Trends Neurosci. *38*, 108–116.
19. Huang, F., Chotiner, J.K., and Steward, O. (2007). Actin polymerization and ERK phosphorylation are required for Arc/Arg3.1 mRNA targeting to activated synaptic sites on dendrites. J. Neurosci. *27*, 9054–9067.
20. Saha, R.N., and Dudek, S.M. (2013). Splitting hares and tortoises: a classification of neuronal immediate early gene transcription based on poised RNA polymerase II. Neuroscience *247*, 175–181.
21. Luescher, C., and Malenka, R.C. (2009). NMDA Receptor-Dependent Long-Term Potentiation and Long-Term Depression (LTP/LTD) Christian. Cold Spring Harb. Perspect. Biol. *4*, a005710.
22. Walkup, W.G., 4th, Sweredoski, M.J., Graham, R.L., Hess, S., and Kennedy, M.B. (2018). Phosphorylation of synaptic GTPase-activating protein (synGAP) by polo-like kinase (Plk2) alters the ratio of its GAP activity toward HRas, Rap1 and Rap2 GTPases. Biochem. Biophys. Res. Commun. *503*, 1599–1604.
23. Sawada, Y., Nakamura, K., Doi, K., Takeda, K., Tobiume, K., Saitoh, M., Morita, K., Komuro, I., De Vos, K., Sheetz, M., and Ichijo, H. (2001). Rap1 is involved in cell stretching modulation of p38 but not ERK or JNK MAP kinase. J. Cell Sci. *114*, 1221–1227.
24. Lee, K.J., Lee, Y., Rozeboom, A., Lee, J.Y., Udagawa, N., Hoe, H.S., and Pak, D.T.S. (2011). Requirement for Plk2 in orchestrated ras and rap signaling, homeostatic structural plasticity, and memory. Neuron *69*, 957–973.
25. Kishore, A., Joseph, T., Velayudhan, B., Popa, T., and Meunier, S. (2012). Early, severe and bilateral loss of LTP and LTD-like plasticity in motor cortex (M1) in de novo Parkinson's disease. Clin. Neurophysiol. *123*, 822–828.
26. Koch, G., Di Lorenzo, F., Bonnì, S., Ponzo, V., Caltagirone, C., and Martorana, A. (2012). Impaired LTP- but not LTD-like cortical plasticity in Alzheimer's disease patients. J. Alzheimers Dis. *31*, 593–599.
27. Kaufman, L., Ayub, M., and Vincent, J.B. (2010). The genetic basis of non-syndromic intellectual disability: a review. J. Neurodev. Disord. *2*, 182–209.
28. Bliss, T.V.P., and Cooke, S.F. (2011). Long-term potentiation and long-term depression: a clinical perspective. Clinics (São Paulo) *66* (*Suppl 1*), 3–17.
29. Gou, G., Roca-Fernandez, A., Kilinc, M., Serrano, E., Reig-Viader, R., Araki, Y., Huganir, R.L., de Quintana-Schmidt, C., Rumbaugh, G., and Bayés, À. (2020). SynGAP splice variants display heterogeneous spatio-temporal expression and subcellular distribution in the developing mammalian brain. J. Neurochem. *154*, 618–634.
30. Vlaskamp, D.R.M., Shaw, B.J., Burgess, R., Mei, D., Montomoli, M., Xie, H., Myers, C.T., Bennett, M.F., XiangWei, W., Williams, D., et al. (2019). *SYNGAP1* encephalopathy: A distinctive generalized developmental and epileptic encephalopathy. Neurology *92*, e96–e107.
31. Parker, M.J., Fryer, A.E., Shears, D.J., Lachlan, K.L., McKee, S.A., Magee, A.C., Mohammed, S., Vasudevan, P.C., Park, S.M., Benoit, V., et al. (2015). De novo, heterozygous, loss-of-function mutations in SYNGAP1 cause a syndromic form of intellectual disability. Am. J. Med. Genet. A. *167A*, 2231–2237.
32. Berryer, M.H., Hamdan, F.F., Klitten, L.L., Møller, R.S., Carmant, L., Schwartzentruber, J., Patry, L., Dobrzeniecka, S., Rochefort, D., Neugnot-Cerioli, M., et al. (2013). Mutations in SYNGAP1 cause intellectual disability, autism, and a specific form of epilepsy by inducing haploinsufficiency. Hum. Mutat. *34*, 385–394.
33. Hamdan, F.F., Gauthier, J., Spiegelman, D., Noreau, A., Yang, Y., Pellerin, S., Dobrzeniecka, S., Côté, M., Perreau-Linck, E., Carmant, L., et al.; Synapse to Disease Group (2009). Mutations in SYNGAP1 in autosomal nonsyndromic mental retardation. N. Engl. J. Med. *360*, 599–605.
34. Clement, J.P., Aceti, M., Creson, T.K., Ozkan, E.D., Shi, Y., Reish, N.J., Almonte, A.G., Miller, B.H., Wiltgen, B.J., Miller, C.A., et al. (2012). Pathogenic SYNGAP1 mutations impair cognitive development by disrupting maturation of dendritic spine synapses. Cell *151*, 709–723.
35. Singh, T., Neale, B., Daly, M.; and Schizophrenia Exome Meta-Analysis Consortium (2019). Initial Results From the Meta-Analysis of the Whole-Exomes of Over 20,000 Schizophrenia Cases and 45,000 Controls. Eur. Neuropsychopharmacol. *29*, S813–S814.
36. Abrahams, B.S., Arking, D.E., Campbell, D.B., Mefford, H.C., Morrow, E.M., Weiss, L.A., Menashe, I., Wadkins, T., Banerjee-Basu, S., and Packer, A. (2013). SFARI Gene 2.0: a community-driven knowledgebase for the autism spectrum disorders (ASDs). Mol. Autism *4*, 36.

37. Kozol, R.A., Cukier, H.N., Zou, B., Mayo, V., De Rubeis, S., Cai, G., Griswold, A.J., Whitehead, P.L., Haines, J.L., Gilbert, J.R., et al. (2015). Two knockdown models of the autism genes SYNGAP1 and SHANK3 in zebrafish produce similar behavioral phenotypes associated with embryonic disruptions of brain morphogenesis. Hum. Mol. Genet. *24*, 4006–4023.
38. Kilinc, M., Creson, T., Rojas, C., Aceti, M., Ellegood, J., Vaissiere, T., Lerch, J.P., and Rumbaugh, G. (2018). Species-conserved SYNGAP1 phenotypes associated with neurodevelopmental disorders. Mol. Cell. Neurosci. *91*, 140–150.
39. Muhia, M., Yee, B.K., Feldon, J., Markopoulos, F., and Knuesel, I. (2010). Disruption of hippocampus-regulated behavioural and cognitive processes by heterozygous constitutive deletion of SynGAP. Eur. J. Neurosci. *31*, 529–543.
40. Guo, X., Hamilton, P.J., Reish, N.J., Sweatt, J.D., Miller, C.A., and Rumbaugh, G. (2009). Reduced expression of the NMDA receptor-interacting protein SynGAP causes behavioral abnormalities that model symptoms of Schizophrenia. Neuropsychopharmacology *34*, 1659–1672.
41. Barnett, M.W., Watson, R.F., Vitalis, T., Porter, K., Komiyama, N.H., Stoney, P.N., Gillingwater, T.H., Grant, S.G.N., and Kind, P.C. (2006). Synaptic Ras GTPase activating protein regulates pattern formation in the trigeminal system of mice. J. Neurosci. *26*, 1355–1365.
42. Kim, J.H., Lee, H.K., Takamiya, K., and Huganir, R.L. (2003). The role of synaptic GTPase-activating protein in neuronal development and synaptic plasticity. J. Neurosci. *23*, 1119–1124.
43. Knuesel, I., Elliott, A., Chen, H.J., Mansuy, I.M., and Kennedy, M.B. (2005). A role for synGAP in regulating neuronal apoptosis. Eur. J. Neurosci. *21*, 611–621.
44. Kopanitsa, M.V., Gou, G., Afinowi, N.O., Bayés, À., Grant, S.G.N., and Komiyama, N.H. (2018). Chronic treatment with a MEK inhibitor reverses enhanced excitatory field potentials in Syngap1$^{+/-}$ mice. Pharmacol. Rep. *70*, 777–783.
45. McGuire, J.L., Depasquale, E.A., Funk, A.J., O'Donnovan, S.M., Hasselfeld, K., Marwaha, S., Hammond, J.H., Hartounian, V., Meador-Woodruff, J.H., Meller, J., and McCullumsmith, R.E. (2017). Abnormalities of signal transduction networks in chronic schizophrenia. NPJ Schizophr. *3*, 30.
46. Balu, D.T. (2016). The NMDA Receptor and Schizophrenia: From Pathophysiology to Treatment. Adv. Pharmacol. *76*, 351–382.
47. Komiyama, N.H., Watabe, A.M., Carlisle, H.J., Porter, K., Charlesworth, P., Monti, J., Strathdee, D.J.C., O'Carroll, C.M., Martin, S.J., Morris, R.G.M., et al. (2002). SynGAP regulates ERK/MAPK signaling, synaptic plasticity, and learning in the complex with postsynaptic density 95 and NMDA receptor. J. Neurosci. *22*, 9721–9732.
48. Nateri, A.S., Raivich, G., Gebhardt, C., Da Costa, C., Naumann, H., Vreugdenhil, M., Makwana, M., Brandner, S., Adams, R.H., Jefferys, J.G.R., et al. (2007). ERK activation causes epilepsy by stimulating NMDA receptor activity. EMBO J. *26*, 4891–4901.
49. Carlisle, H.J., Manzerra, P., Marcora, E., and Kennedy, M.B. (2008). SynGAP regulates steady-state and activity-dependent phosphorylation of cofilin. J. Neurosci. *28*, 13673–13683.
50. Rumbaugh, G., Adams, J.P., Kim, J.H., and Huganir, R.L. (2006). SynGAP regulates synaptic strength and mitogen-activated protein kinases in cultured neurons. Proc. Natl. Acad. Sci. USA *103*, 4344–4351.
51. Vazquez, L.E., Chen, H.J., Sokolova, I., Knuesel, I., and Kennedy, M.B. (2004). SynGAP regulates spine formation. J. Neurosci. *24*, 8862–8872.
52. Beurel, E., Grieco, S.F., and Jope, R.S. (2015). Glycogen synthase kinase-3 (GSK3): regulation, actions, and diseases. Pharmacol. Ther. *148*, 114–131.
53. Hur, E.M., and Zhou, F.Q. (2010). GSK3 signalling in neural development. Nat. Rev. Neurosci. *11*, 539–551.
54. Bradley, C.A., Peineau, S., Taghibiglou, C., Nicolas, C.S., Whitcomb, D.J., Bortolotto, Z.A., Kaang, B.K., Cho, K., Wang, Y.T., and Collingridge, G.L. (2012). A pivotal role of GSK-3 in synaptic plasticity. Front. Mol. Neurosci. *5*, 13.
55. Seo, M.S., Kim, S.H., Ahn, Y.M., Kim, Y., Jeon, W.J., Yoon, S.C., Roh, M.S., Juhnn, Y.S., and Kim, Y.S. (2007). The effects of repeated administrations of MK-801 on ERK and GSK-3β signalling pathways in the rat frontal cortex. Int. J. Neuropsychopharmacol. *10*, 359–368.
56. Li, L., Fan, Y., Huang, X., Luo, J., Zhong, L., Shu, X.S., Lu, L., Xiang, T., Chan, A.T.C., Yeo, W., et al. (2019). Tumor Suppression of Ras GTPase-Activating Protein RASA5 through Antagonizing Ras Signaling Perturbation in Carcinomas. iScience *21*, 1–18.
57. Whiffin, N., Roberts, A.M., Minikel, E., Zappala, Z., Walsh, R., O'Donnell-Luria, A.H., Karczewski, K.J., Harrison, S.M., Thomson, K.L., Sage, H., et al. (2019). Using High-Resolution Variant Frequencies Empowers Clinical Genome Interpretation and Enables Investigation of Genetic Architecture. Am. J. Hum. Genet. *104*, 187–190.
58. Leblond, C.S., Cliquet, F., Carton, C., Huguet, G., Mathieu, A., Kergrohen, T., Buratti, J., Lemière, N., Cuisset, L., Bienvenu, T., et al. (2019). Both rare and common genetic variants contribute to autism in the Faroe Islands. NPJ Genom. Med. *4*, 1–10.
59. Iossifov, I., Levy, D., Allen, J., Ye, K., Ronemus, M., Lee, Y.H., Yamrom, B., and Wigler, M. (2015). Low load for disruptive mutations in autism genes and their biased transmission. Proc. Natl. Acad. Sci. USA *112*, E5600–E5607.
60. Grove, J., Ripke, S., Als, T.D., Mattheisen, M., Walters, R.K., Won, H., Pallesen, J., Agerbo, E., Andreassen, O.A., Anney, R., et al.; Autism Spectrum Disorder Working Group of the Psychiatric Genomics Consortium; BUPGEN; Major Depressive Disorder Working Group of the Psychiatric Genomics Consortium; and 23andMe Research Team (2019). Identification of common genetic risk variants for autism spectrum disorder. Nat. Genet. *51*, 431–444.
61. Bölte, S., Girdler, S., and Marschik, P.B. (2019). The contribution of environmental exposure to the etiology of autism spectrum disorder. Cell. Mol. Life Sci. *76*, 1275–1297.
62. Clarke, T.K., Lupton, M.K., Fernandez-Pujals, A.M., Starr, J., Davies, G., Cox, S., Pattie, A., Liewald, D.C., Hall, L.S., MacIntyre, D.J., et al. (2016). Common polygenic risk for autism spectrum disorder (ASD) is associated with cognitive ability in the general population. Mol. Psychiatry *21*, 419–425.
63. Richards, S., Aziz, N., Bale, S., Bick, D., Das, S., Gastier-Foster, J., Grody, W.W., Hegde, M., Lyon, E., Spector, E., et al.; ACMG Laboratory Quality Assurance Committee (2015). Standards and guidelines for the interpretation of sequence variants: a joint consensus recommendation of the American College of Medical Genetics and Genomics and the Association for Molecular Pathology. Genet. Med. *17*, 405–424.
64. Brnich, S.E., Abou Tayoun, A.N., Couch, F.J., Cutting, G.R., Greenblatt, M.S., Heinen, C.D., Kanavy, D.M., Luo, X.,

Mcnulty, S.M., Starita, L.M., et al. (2020). Recommendations for application of the functional evidence PS3/BS3 criterion using the ACMG/AMP sequence variant interpretation framework On behalf of the Clinical Genome Resource Sequence Variant Interpretation Working Group. Genome Med. *12*. https://doi.org/10.1186/s13073-019-0690-2.

65. Post, K.L., Belmadani, M., Ganguly, P., Meili, F., Dingwall, R., McDiarmid, T.A., Meyers, W.M., Herrington, C., Young, B.P., Callaghan, D.B., et al. (2020). Multi-model functionalization of disease-associated PTEN missense mutations identifies multiple molecular mechanisms underlying protein dysfunction. Nat. Commun. *11*, 2073.
66. Mighell, T.L., Evans-Dutson, S., and O'Roak, B.J. (2018). A Saturation Mutagenesis Approach to Understanding PTEN Lipid Phosphatase Activity and Genotype-Phenotype Relationships. Am. J. Hum. Genet. *102*, 943–955.
67. Yi, S., Liu, N.N., Hu, L., Wang, H., and Sahni, N. (2017). Base-resolution stratification of cancer mutations using functional variomics. Nat. Protoc. *12*, 2323–2341.
68. Bill, A., Popa, M.O., van Diepen, M.T., Gutierrez, A., Lilley, S., Velkova, M., Acheson, K., Choudhury, H., Renaud, N.A., Auld, D.S., et al. (2015). Variomics screen identifies the re-entrant loop of the calcium-activated chloride channel ANO1 that facilitates channel activation. J. Biol. Chem. *290*, 889–903.
69. Matreyek, K.A., Starita, L.M., Stephany, J.J., Martin, B., Chiasson, M.A., Gray, V.E., Kircher, M., Khechaduri, A., Dines, J.N., Hause, R.J., et al. (2018). Multiplex assessment of protein variant abundance by massively parallel sequencing. Nat. Genet. *50*, 874–882.
70. Karczewski, K.J., Francioli, L.C., Tiao, G., Cummings, B.B., Alföldi, J., Wang, Q., Collins, R.L., Laricchia, K.M., Ganna, A., Birnbaum, D.P., et al.; Genome Aggregation Database Consortium (2020). The mutational constraint spectrum quantified from variation in 141,456 humans. Nature *581*, 434–443.
71. Landrum, M.J., Lee, J.M., Benson, M., Brown, G.R., Chao, C., Chitipiralla, S., Gu, B., Hart, J., Hoffman, D., Jang, W., et al. (2018). ClinVar: improving access to variant interpretations and supporting evidence. Nucleic Acids Res. *46* (D1), D1062–D1067.
72. Belmadani, M., Jacobson, M., Holmes, N., Phan, M., Nguyen, T., Pavlidis, P., and Rogic, S. (2019). VariCarta: A Comprehensive Database of Harmonized Genomic Variants Found in Autism Spectrum Disorder Sequencing Studies. Autism Res. *12*, 1728–1736.
73. McRae, J.F., Clayton, S., Fitzgerald, T.W., Kaplanis, J., Prigmore, E., Rajan, D., Sifrim, A., Aitken, S., Akawi, N., Alvi, M., et al.; Deciphering Developmental Disorders Study (2017). Prevalence and architecture of de novo mutations in developmental disorders. Nature *542*, 433–438.
74. C Yuen, R.K., Merico, D., Bookman, M., L Howe, J., Thiruvahindrapuram, B., Patel, R.V., Whitney, J., Deflaux, N., Bingham, J., Wang, Z., et al. (2017). Whole genome sequencing resource identifies 18 new candidate genes for autism spectrum disorder. Nat. Neurosci. *20*, 602–611.
75. Codina-Solà, M., Rodríguez-Santiago, B., Homs, A., Santoyo, J., Rigau, M., Aznar-Laín, G., Del Campo, M., Gener, B., Gabau, E., Botella, M.P., et al. (2015). Integrated analysis of whole-exome sequencing and transcriptome profiling in males with autism spectrum disorders. Mol. Autism *6*, 21.
76. De Rubeis, S., He, X., Goldberg, A.P., Poultney, C.S., Samocha, K., Cicek, A.E., Kou, Y., Liu, L., Fromer, M., Walker, S., et al.; DDD Study; Homozygosity Mapping Collaborative for Autism; and UK10K Consortium (2014). Synaptic, transcriptional and chromatin genes disrupted in autism. Nature *515*, 209–215.
77. Fieremans, N., Van Esch, H., Holvoet, M., Van Goethem, G., Devriendt, K., Rosello, M., Mayo, S., Martinez, F., Jhangiani, S., Muzny, D.M., et al. (2016). Identification of Intellectual Disability Genes in Female Patients with a Skewed X-Inactivation Pattern. Hum. Mutat. *37*, 804–811.
78. Kosmicki, J.A., Samocha, K.E., Howrigan, D.P., Sanders, S.J., Slowikowski, K., Lek, M., Karczewski, K.J., Cutler, D.J., Devlin, B., Roeder, K., et al. (2017). Refining the role of de novo protein-truncating variants in neurodevelopmental disorders by using population reference samples. Nat. Genet. *49*, 504–510.
79. Brett, M., McPherson, J., Zang, Z.J., Lai, A., Tan, E.S., Ng, I., Ong, L.C., Cham, B., Tan, P., Rozen, S., and Tan, E.C. (2014). Massively parallel sequencing of patients with intellectual disability, congenital anomalies and/or autism spectrum disorders with a targeted gene panel. PLoS ONE *9*, e93409.
80. Stessman, H.A.F., Xiong, B., Coe, B.P., Wang, T., Hoekzema, K., Fenckova, M., Kvarnung, M., Gerdts, J., Trinh, S., Cosemans, N., et al. (2017). Targeted sequencing identifies 91 neurodevelopmental-disorder risk genes with autism and developmental-disability biases. Nat. Genet. *49*, 515–526.
81. Ahmadian, M.R., Kiel, C., Stege, P., and Scheffzek, K. (2003). Structural fingerprints of the Ras-GTPase activating proteins neurofibromin and p120GAP. J. Mol. Biol. *329*, 699–710.
82. Araki, Y., Hong, I., Gamache, T.R., Ju, S., Collado-Torres, L., Shin, J.H., and Huganir, R.L. (2020). SynGAP isoforms differentially regulate synaptic plasticity and dendritic development. eLife *9*, 9.
83. McQuin, C., Goodman, A., Chernyshev, V., Kamentsky, L., Cimini, B.A., Karhohs, K.W., Doan, M., Ding, L., Rafelski, S.M., Thirstrup, D., et al. (2018). CellProfiler 3.0: Next-generation image processing for biology. PLoS Biol. *16*, e2005970.
84. Ding, Q., Xia, W., Liu, J.C., Yang, J.Y., Lee, D.F., Xia, J., Bartholomeusz, G., Li, Y., Pan, Y., Li, Z., et al. (2005). Erk associates with and primes GSK-3β for its inactivation resulting in upregulation of β-catenin. Mol. Cell *19*, 159–170.
85. Ollila, S., Dermadi Bebek, D., Jiricny, J., and Nyström, M. (2008). Mechanisms of pathogenicity in human MSH2 missense mutants. Hum. Mutat. *29*, 1355–1363.
86. Henderson, D.M., Lee, A., and Ervasti, J.M. (2010). Disease-causing missense mutations in actin binding domain 1 of dystrophin induce thermodynamic instability and protein aggregation. Proc. Natl. Acad. Sci. USA *107*, 9632–9637.
87. Walton, M., Woodgate, A.M., Muravlev, A., Xu, R., During, M.J., and Dragunow, M. (1999). CREB phosphorylation promotes nerve cell survival. J. Neurochem. *73*, 1836–1842.
88. Wang, H., Xu, J., Lazarovici, P., Quirion, R., and Zheng, W. (2018). cAMP Response Element-Binding Protein (CREB): A Possible Signaling Molecule Link in the Pathophysiology of Schizophrenia. Front. Mol. Neurosci. *11*, 255.
89. Wlodkowic, D., Telford, W., Skommer, J., and Darzynkiewicz, Z. (2011). Apoptosis and beyond: cytometry in studies of programmed cell death. Methods Cell Biol. *103*, 55–98.
90. Walton, M.R., and Dragunow, I. (2000). Is CREB a key to neuronal survival? Trends Neurosci. *23*, 48–53.

91. Lonze, B.E., Riccio, A., Cohen, S., and Ginty, D.D. (2002). Apoptosis, axonal growth defects, and degeneration of peripheral neurons in mice lacking CREB. Neuron *34*, 371–385.
92. Zeng, M., Shang, Y., Araki, Y., Guo, T., Huganir, R.L., and Zhang, M. (2016). Phase Transition in Postsynaptic Densities Underlies Formation of Synaptic Complexes and Synaptic Plasticity. Cell *166*, 1163–1175.e12.
93. Steven, A., and Seliger, B. (2016). Control of CREB expression in tumors: from molecular mechanisms and signal transduction pathways to therapeutic target. Oncotarget *7*, 35454–35465.
94. Watson, F.L., Heerssen, H.M., Bhattacharyya, A., Klesse, L., Lin, M.Z., and Segal, R.A. (2001). Neurotrophins use the Erk5 pathway to mediate a retrograde survival response. Nat. Neurosci. *4*, 981–988.
95. Watson, F.L., Heerssen, H.M., Moheban, D.B., Lin, M.Z., Sauvageot, C.M., Bhattacharyya, A., Pomeroy, S.L., and Segal, R.A. (1999). Rapid nuclear responses to target-derived neurotrophins require retrograde transport of ligand-receptor complex. J. Neurosci. *19*, 7889–7900.
96. Riccio, A., Pierchala, B.A., Ciarallo, C.L., and Ginty, D.D. (1997). An NGF-TrkA-mediated retrograde signal to transcription factor CREB in sympathetic neurons. Science *277*, 1097–1100.
97. Cox, L.J., Hengst, U., Gurskaya, N.G., Lukyanov, K.A., and Jaffrey, S.R. (2008). Intra-axonal translation and retrograde trafficking of CREB promotes neuronal survival. Nat. Cell Biol. *10*, 149–159.
98. Crino, P., Khodakhah, K., Becker, K., Ginsberg, S., Hemby, S., and Eberwine, J. (1998). Presence and phosphorylation of transcription factors in developing dendrites. Proc. Natl. Acad. Sci. USA *95*, 2313–2318.
99. Redmond, L., Kashani, A.H., and Ghosh, A. (2002). Calcium regulation of dendritic growth via CaM kinase IV and CREB-mediated transcription. Neuron *34*, 999–1010.
100. Naguib, A., Bencze, G., Cho, H., Zheng, W., Tocilj, A., Elkayam, E., Faehnle, C.R., Jaber, N., Pratt, C.P., Chen, M., et al. (2015). PTEN functions by recruitment to cytoplasmic vesicles. Mol. Cell *58*, 255–268.
101. Medkova, M., and Cho, W. (1998). Mutagenesis of the C2 domain of protein kinase C-α. Differential roles of Ca2+ ligands and membrane binding residues. J. Biol. Chem. *273*, 17544–17552.
102. Corbalan-Garcia, S., and Gómez-Fernández, J.C. (2014). Signaling through C2 domains: more than one lipid target. Biochim. Biophys. Acta *1838*, 1536–1547.
103. Nalefski, E.A., and Falke, J.J. (1996). The C2 domain calcium-binding motif: structural and functional diversity. Protein Sci. *5*, 2375–2390.
104. Cho, W., and Stahelin, R.V. (2006). Membrane binding and subcellular targeting of C2 domains. Biochim. Biophys. Acta *1761*, 838–849.
105. Babu, M.M., van der Lee, R., de Groot, N.S., and Gsponer, J. (2011). Intrinsically disordered proteins: regulation and disease. Curr. Opin. Struct. Biol. *21*, 432–440.
106. Garza, A.S., Ahmad, N., and Kumar, R. (2009). Role of intrinsically disordered protein regions/domains in transcriptional regulation. Life Sci. *84*, 189–193.
107. Patil, A., and Nakamura, H. (2006). Disordered domains and high surface charge confer hubs with the ability to interact with multiple proteins in interaction networks. FEBS Lett. *580*, 2041–2045.
108. Watson, M.D., Monroe, J., and Raleigh, D.P. (2018). Size-Dependent Relationships between Protein Stability and Thermal Unfolding Temperature Have Important Implications for Analysis of Protein Energetics and High-Throughput Assays of Protein-Ligand Interactions. J. Phys. Chem. B *122*, 5278–5285.
109. Lee, D.Y., Kim, K.A., Yu, Y.G., and Kim, K.S. (2004). Substitution of aspartic acid with glutamic acid increases the unfolding transition temperature of a protein. Biochem. Biophys. Res. Commun. *320*, 900–906.
110. Yang, J.M., Nam, K., Kim, H.C., Lee, J.H., Park, J.K., Wu, K., Lee, E.S., and Steinert, P.M. (1999). A novel glutamic acid to aspartic acid mutation near the end of the 2B rod domain in the keratin 1 chain in epidermolytic hyperkeratosis. J. Invest. Dermatol. *112*, 376–379.
111. McMahon, A.C., Barnett, M.W., O'Leary, T.S., Stoney, P.N., Collins, M.O., Papadia, S., Choudhary, J.S., Komiyama, N.H., Grant, S.G.N., Hardingham, G.E., et al. (2012). SynGAP isoforms exert opposing effects on synaptic strength. Nat. Commun. *3*, 900.
112. Grimm, D.G., Azencott, C.A., Aicheler, F., Gieraths, U., MacArthur, D.G., Samocha, K.E., Cooper, D.N., Stenson, P.D., Daly, M.J., Smoller, J.W., et al. (2015). The evaluation of tools used to predict the impact of missense variants is hindered by two types of circularity. Hum. Mutat. *36*, 513–523.
113. Miller, M., Bromberg, Y., and Swint-Kruse, L. (2017). Computational predictors fail to identify amino acid substitution effects at rheostat positions. Sci. Rep. *7*, 41329.
114. MacArthur, D.G., Balasubramanian, S., Frankish, A., Huang, N., Morris, J., Walter, K., Jostins, L., Habegger, L., Pickrell, J.K., Montgomery, S.B., et al.; 1000 Genomes Project Consortium (2012). A systematic survey of loss-of-function variants in human protein-coding genes. Science *335*, 823–828.
115. MacArthur, D.G., and Tyler-Smith, C. (2010). Loss-of-function variants in the genomes of healthy humans. Hum. Mol. Genet. *19* (R2), R125–R130.